



Deciphering Functional Connectivity Differences Between Motor Imagery and Execution of Target-Oriented Grasping

Eunkyung Kim^{1,2} · Woo Hyung Lee^{1,3,4} · Han Gil Seo^{1,4} · Hyung Seok Nam^{1,3,4} · Yoon Jae Kim⁵ · Min-Gu Kang¹ · Moon Suk Bang^{1,4,6} · Sungwan Kim^{3,7} · Byung-Mo Oh^{1,4,6,8}

Received: 21 August 2022 / Accepted: 20 March 2023 / Published online: 15 April 2023
© The Author(s), under exclusive licence to Springer Science+Business Media, LLC, part of Springer Nature 2023

Abstract

This study aimed to delineate overlapping and distinctive functional connectivity in visual motor imagery, kinesthetic motor imagery, and motor execution of target-oriented grasping action of the right hand. Functional magnetic resonance imaging data were obtained from 18 right-handed healthy individuals during each condition. Seed-based connectivity and multi-voxel pattern analyses were employed after selecting seed regions with the left primary motor cortex and supplementary motor area. There was equivalent seed-based connectivity during the three conditions in the bilateral frontoparietal and temporal areas. When the seed region was the left primary motor cortex, increased connectivity was observed in the left cuneus and superior frontal area during visual and kinesthetic motor imageries, respectively, compared with that during motor execution. Multi-voxel pattern analyses revealed that each condition was differentiated by spatially distributed connectivity patterns of the left primary motor cortex within the right cerebellum VI, cerebellum crus II, and left lingual area. When the seed region was the left supplementary motor area, the connectivity patterns within the right putamen, thalamus, cerebellar areas IV-V, and left superior parietal lobule were significantly classified above chance level across the three conditions. The present findings improve our understanding of the spatial representation of functional connectivity and its specific patterns among motor imagery and motor execution. The strength and fine-grained connectivity patterns of the brain areas can discriminate between motor imagery and motor execution.

Keywords Cerebellum · Mental Processes · Motor Cortex · Motor Imagery · Multi-voxel pattern analysis · Occipital Lobe

Eunkyung Kim and Woo Hyung Lee equally contributed as co-first authors.

Sungwan Kim and Byung-Mo Oh share last authorship.

Handling Editor: Francesco DE PASQUALE

✉ Sungwan Kim
sungwan@snu.ac.kr

✉ Byung-Mo Oh
moyal@snu.ac.kr

¹ Department of Rehabilitation Medicine, Seoul National University Hospital, Seoul, Republic of Korea

² Biomedical Research Institute, Seoul National University Hospital, Seoul, Republic of Korea

³ Department of Biomedical Engineering, Seoul National University College of Medicine, Seoul, Republic of Korea

⁴ Department of Rehabilitation Medicine, Seoul National University College of Medicine, Seoul, Republic of Korea

⁵ Institute of Medical and Biological Engineering, Medical Research Center, Seoul National University, Seoul, Republic of Korea

⁶ National Traffic Injury Rehabilitation Hospital, Yangpyeong, Republic of Korea

⁷ Institute of Bioengineering, Seoul National University, Seoul, Republic of Korea

⁸ Institute on aging, Seoul National University, Seoul, Republic of Korea

Introduction

As a dynamic mental state, motor imagery is an internally rehearsed motor act without an overt motor output (Decety 1996). Neuroimaging studies have revealed a functional equivalence between motor imagery and actual motor execution (ME), sharing similar brain physiological characteristics (Grezes and Decety 2001; Hetu et al. 2013; Jeannerod 1994). Similar motor-related brain activity was observed during motor imagery and ME, including in the frontoparietal cortex and cerebellum (Hanakawa et al. 2003; Hetu et al. 2013) and subcortical areas of the brain (Grezes and Decety 2001; Hetu et al. 2013). Conversely, a different neural activity was observed during motor imagery and ME (Guillot et al. 2009; Lee et al. 2019). In particular, the premotor regions, inferior and superior parietal cortices were more activated during motor imagery than during ME (Hardwick et al. 2018). The specific representation of neural activity and similar brain activation characterizes the neural substrates of motor imagery distinctive to those of ME.

Motor imagery training has been used to improve motor performance in numerous fields based on the understanding of equivalent functional systems between motor imagery and ME in the brain (Ladda et al. 2021). From a practical perspective, target-oriented motor imagery is important since the target-oriented movement is essential in accomplishing successful movements during numerous daily activities and in brain-computer interfaces and sport sciences (Daly and Wolpaw 2008; Mokienko, Chernikova, Frolov, & Bobrov, 2014). The primary motor area (M1), one of the core brain regions during motor tasks, is activated during target-oriented movement to execute voluntary actions (Scott 2003). The region is involved in the somatomotor network responsible for motor sequence processing, planning, and executing movements (Gallese and Lakoff 2005), activated during motor imagery and ME (Hanakawa et al. 2005), and interconnected with various brain areas to form the motor network (Guye et al. 2003). Therefore, it would be interesting to know how the brain regions are interconnected during motor imagery and ME, particularly focusing on the M1 as a seed region. Previous studies have investigated the causal relationship between the M1 and other brain areas confined to motor-related regions during motor imagery and ME (Chen et al. 2009; Q. Gao, Duan, & Chen, 2011; Y. Kim, Park, Lee, Im, & Kim, 2018; Solodkin, Hlustik, Chen, & Small, 2004). However, the similarity and difference in functional connectivity of the M1 during target-oriented motor imagery and ME are yet to be investigated.

In general, seed-based functional connectivity considers the interactions between the seed and various regions of the brain, typically in voxels, independently; it does not consider spatial complexity or organization of the brain.

Examining spatial distribution of voxel-level variability in the brain signal during target-oriented actions is important as spatially neighboring neural activities are systematically organized in the brain (Silver and Kastner 2009). In this regard, multi-voxel pattern analysis (MVPA) can be useful for evaluating voxel-level variability (Davis et al. 2014) by analyzing the patterns of functional connectivity (Dosenbach et al. 2010; Liu et al. 2015). It can allow motor imagery and ME to be distinguished by considering the spatial information of the neural interrelationship. Previous studies have decoded motor imagery and ME using the spatial patterns of brain signals, by taking pre-determined ROIs, including the M1 (Pilgramm et al. 2016; Zabicki et al. 2017). More reliable information could be obtained using the spatial patterns of functional connectivity of the M1 with the whole-brain areas.

The present study aimed to investigate M1-based functional connectivity during target-oriented motor imagery and ME and examine how these functional networks are equivalent or different, specifically focusing on visual motor imagery (V-I), kinesthetic motor imagery (K-I), and ME in healthy individuals. In addition, this study aimed to examine the supplementary motor area (SMA)-based functional connectivity during each condition, which is one of the important hub regions within the somatomotor network modulating internal motor preparation and control of self-initiated movements (Cunnington et al. 2002). We also sought to identify the connectivity patterns that discriminate V-I, K-I, and ME using the MVPA approach. Functional connectivity of the brain during different type of motor imagery and ME could involve similar brain areas with different strengths or patterns.

Materials and Methods

The current study included the results of additional analyses on data from a previously published functional magnetic resonance imaging (fMRI) study (Lee et al. 2019) that investigated the distinct characteristics of brain activity during different subtypes of target-oriented motor imagery and ME.

Participants

Of the 20 healthy right-handed volunteers, 18 participants (9 men, mean age: 30.3 ± 4.3 years) without neurological or psychiatric disorders were recruited. Two participants were excluded from further experiments or analyses: one performed K-I incorrectly and the other had a suggestive structural abnormality in the brain. For further information

on the methods, please refer to our previous paper (Lee et al. 2019). This study was approved by the Institutional Review Board. All participants provided written informed consent according to institutional guidelines and regulations. The study was conducted in line with the principles of the Declaration of Helsinki.

Motor Imagery Training Before fMRI

The participants were trained in ME, V-I, and K-I, with each training lasting 15 min. The training task involved grasping and releasing a target object (a green rubber ball) with the right hand at 4-s intervals. During the training sessions, video images were provided as a guide for participants, including the shape, size, and color of the target object, although participants were encouraged to perform and imagine hand grasping and releasing with their eyes closed, as they would during fMRI scanning protocol. The training videos were from a first-person point of view (Lee et al. 2019). During ME, participants performed the actual task by grasping and releasing the target object with their right hand. During V-I, participants were instructed to concentrate on the visual images of grasping and releasing the target object. During K-I, participants were instructed to concentrate on the kinesthetic sensation of the finger joint bending and stretching toward the target object.

Task Design for the fMRI Experiment

An experimental block-design paradigm was presented using the Presentation software package (Neurobehavioral Systems, Davis, CA; <http://www.neurobs.com>; Fig. 1). The experimental paradigm was arranged as follows. In a counterbalanced order, five runs were organized into seven task blocks per run. A task block consisted of five trials, each of which involved one of five different task conditions and lasted 20 s so that each task condition was performed five times per block. The five task conditions were (1) V-I from the first-person perspective, (2) K-I from the first-person perspective, (3) V-I from the third-person perspective, (4) ME, and (5) perceptual control. Of the five conditions, we selectively analyzed functional connectivity during three conditions including V-I from the first-person perspective, K-I from the first-person perspective, and ME with own bodies, focusing on self-initiated target-oriented movement. Four out of five task conditions were used per run, and each task condition was presented seven times as a block during the five runs. There was a resting block of 15 s between the task blocks. During the experiment, auditory stimuli of high-pitched (1500 Hz) and low-pitched (800 Hz) sounds were delivered to the participants binaurally via a headset. The sounds indicated when they should open their eyes to see the task instrument and when to perform the task every 4 s. Specifically, during all task blocks, except the perceptual control, the participants repeated each task five times in response to the low-pitch sounds. During the perceptual

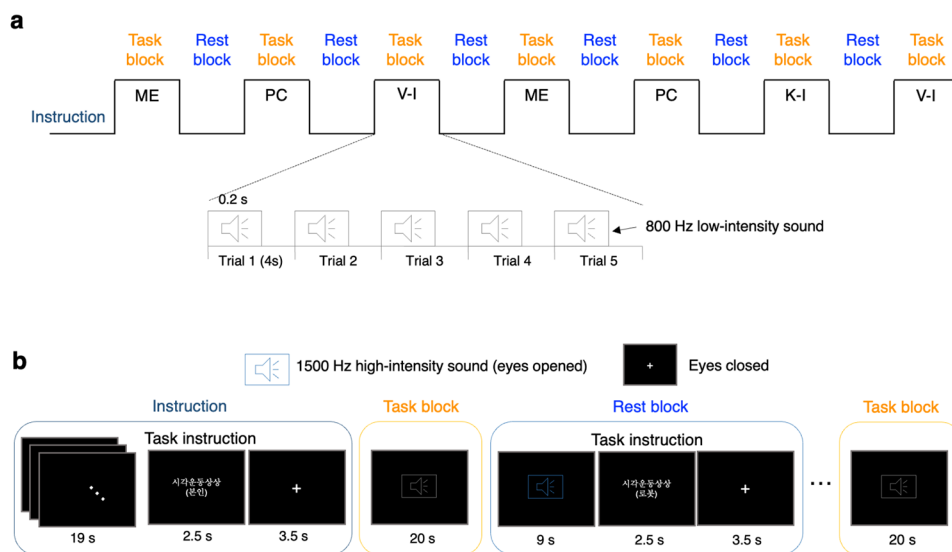


Fig. 1 Experimental design for the task-based functional magnetic resonance imaging study: **a** Schematic representation of visual motor imagery (V-I), kinesthetic motor imagery (K-I), and motor execution (ME). **b** Temporal structure of one example run. Each participant completed five runs organized into seven task blocks in a counterbalanced order. Each task block consisted of five trials, each of which

involved one of five different task conditions. During the task blocks, low-intensity auditory stimuli were delivered to the participants via a headset as a signal to perform the task every 4 s. During rest blocks, high-intensity auditory stimuli were delivered to indicate when the participants should open their eyes to see the task instrument. Notably, the perceptual control (PC) condition was not included in the analysis.

control condition, the participant performed no task but only listened to low-pitch sounds, which were repeated five times. Visual instructions were delivered using a back-projection screen. Before scanning, each participant was familiarized with the experimental setting. Awakeness and experimental errors of the participants were checked case-by-case during short breaks between runs that lasted for 3 min.

Image Acquisition and Preprocessing

The fMRI data were acquired using a 3-T scanner (Siemens Magnetom Trio Tim, Erlangen, Germany) with a 12-channel head coil. A total of 84 T2*-weighted, single-shot, gradient-echo planar image volumes were obtained via axial acquisition of 42 slices per volume, with interleaved acquisition in each run (matrix size = $128 \times 128 \text{ mm}^2$, voxel size = $1.9 \text{ mm} \times 1.9 \text{ mm} \times 3.5 \text{ mm}$, repetition time = 3,000 ms, echo time = 30 ms, field of view = 240 mm, flip angle = 90°). High-resolution structural T1 data were acquired via sagittal acquisition of 208 slices using the 3-D Turbo-FLASH sequence (matrix size = $256 \times 256 \text{ mm}^2$, voxel size = 1 mm^3 , repetition time = 1,670 ms, echo time = 1.89 ms, field of view = 250 mm, flip angle = 9°).

The fMRI data were preprocessed using statistical parametric mapping (SPM12; <http://www.fil.ion.ucl.ac.uk/spm/software/spm12/>). Details of the preprocessing procedure have been presented in our previous study (Lee et al. 2019). Briefly, we applied slice timing correction, realignment and reslicing, spatial normalization (using a deformation map acquired by segmentation of T1 images from a co-registered individual with a mean fMRI image), and smoothing of the normalized fMRI data with an 8-mm full-width at half-maximum Gaussian kernel to increase the signal-to-noise ratio.

Signal contamination due to relatively slight head movements in fMRI is an important issue because it can increase false-positive rates (Friston et al. 1996). Fluctuations in the brain signal and head movements during scanning were detected using the artifact detection toolbox (ART; <https://gablab.mit.edu/index.php/software>). Of the 18 participants, only seven showed outlier volumes in which the scan-to-scan differences in global brain signal, normalized to z-scores, were greater than five and head movement was greater than 2 mm. We did not exclude outlier volumes because the total proportion was only 0.33% (25 out of 7560 volumes—84 volumes \times 5 runs \times 18 participants).

Construction and Comparison of the Seed-Based Functional Connectivity Maps

Seed-based functional connectivity during each condition was constructed and compared using the functional connectivity toolbox (CONN) (<https://www.nitrc.org/projects/conn>; version 18.a) (Whitfield-Gabrieli and Nieto-Castanon 2012). A component-based noise correction strategy (CompCor) was applied (Behzadi et al. 2007) to reduce the effects of nuisance variables. It defines voxels with a signal presumably of no interest, such as white matter and cerebrospinal fluid (Power et al. 2015). A principal component analysis was performed using CompCor to obtain nuisance variables from the voxelwise signals of no interest (Power et al. 2015). Then, the following parameters were estimated and used as covariates in the first-level analysis with a general linear model: the five principal components of white matter and cerebrospinal fluid estimated from the CompCor, where temporal fluctuations are unlikely to be modulated by neural activity, the six motion parameters and their first-order derivatives (i.e., realignment parameter noise), and the main task effects. Data were linearly detrended and bandpass filtered at 0.008–0.09 Hz.

In the previous group-level analysis, the left M1 was one of the brain areas showing significantly greater brain activity during ME than during perceptual control (Lee et al. 2019). We used a more stringent statistical significance threshold to redefine the left M1 (family-wise error (FWE) rate corrected $P < 0.05$) as accurately as possible. The left SMA was also defined by reanalyzing previous findings (Lee et al. 2019) that showed significantly greater brain activity during ME than during perceptual control (uncorrected $P < 0.0005$). Temporal correlations between the averaged blood-oxygen-level-dependent signal of the left M1 and whole-brain voxels and between the signal of the left SMA and whole-brain voxels were computed for each condition, with age as a nuisance variable. The values were then weighted for hemodynamic response function and converted to z-scores by Fisher transformation to improve the normality assumption. To identify the shared brain connectivity of the three conditions, conjunction analyses with minimum statistic (Nichols et al. 2005) were performed among (1) the V-I, K-I, and ME conditions; (2) the V-I and ME conditions; (3) the K-I and ME conditions; and (4) the V-I and K-I conditions. A two-sample *t*-test was performed to ascertain significant differences between V-I and ME, between K-I and ME, and between V-I and K-I. Statistical significance was set at an uncorrected $P < 0.001$, with the cluster-based, FWE rate set at a corrected $P < 0.05$ (Friston et al. 1994).

MVPA

An MVPA was conducted to discriminate patterns of seed-based functional connectivity elicited by V-I, K-I, and ME in an ROI-based approach. A schematic representation of the MVPA is shown in Fig. 2, describing patterns of left M1-based functional connectivity. Step 1: left M1-based

functional connectivity was constructed as a matrix for each subject, represented as conditions-by-whole brain voxels (Fig. 2a). Because each condition had seven task blocks in this study, a matrix consisting of 21-by-whole brain voxels was generated in each subject. The elements of the connectivity matrix were z-values representing the connectivity strength. Step 2: within the connectivity matrix,

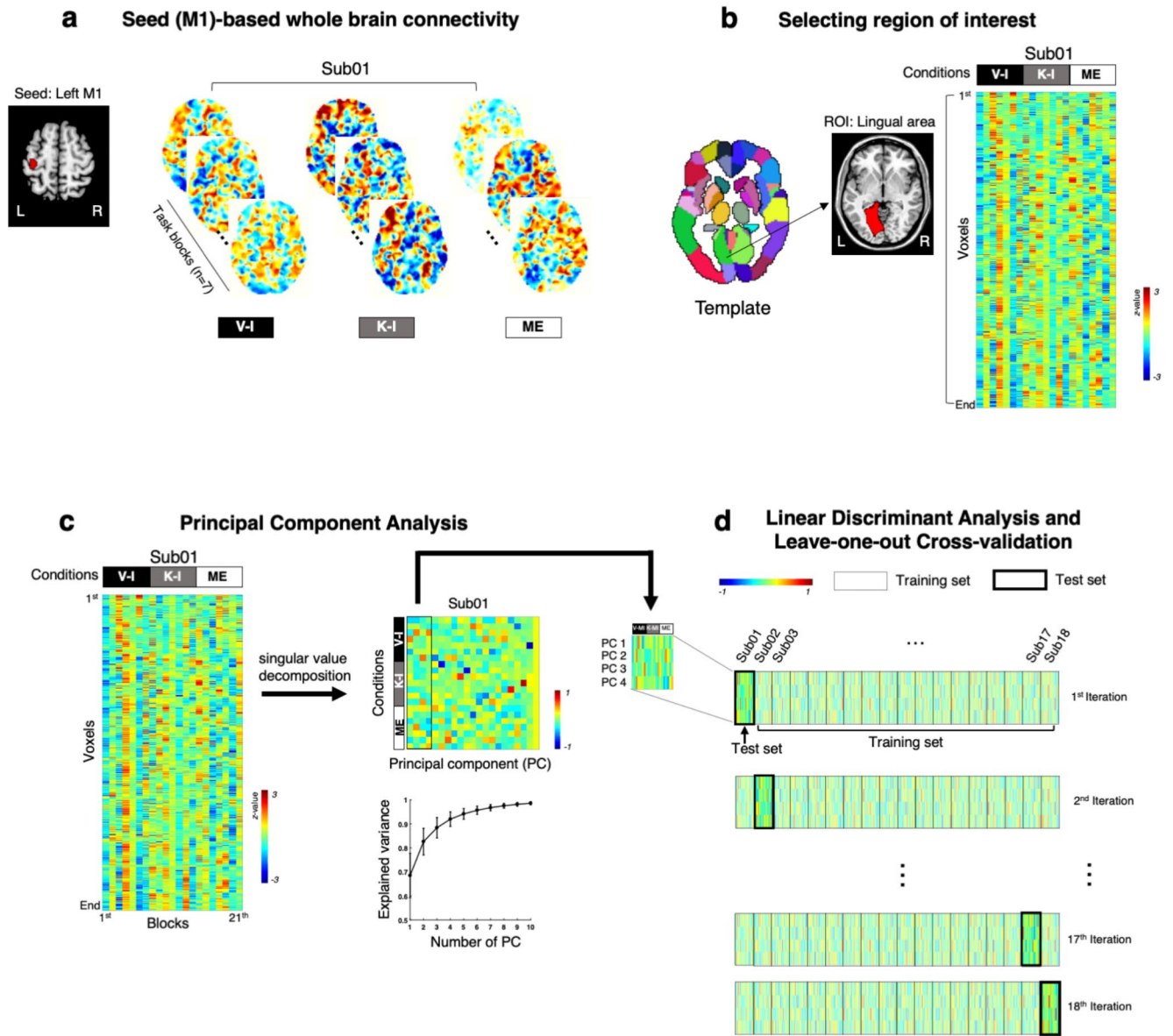


Fig. 2 Schematic illustrations of multi-voxel pattern analysis in a representative case. **a** The left primary motor cortex was used as a seed region to construct seed-based functional connectivity with the whole-brain area during visual motor imagery (V-I), kinesthetic motor imagery (K-I), and motor execution (ME). Because each task condition was presented seven times as a block in this study, 21-whole-brain functional connectivity was generated in each individual. **b** In this schematic representation, functional connectivity observed within the left lingual area was selected to narrow the focus of the analysis. Therefore, a number of voxels within the left lingual area-by-21 matrix

was generated in each individual. The region of interest was determined using the automated anatomical labeling template. **c** Using principal component analysis, the correlation coefficients were calculated between conditions and principal components, so-called loadings, explaining the information they shared. In the line graph, the black dot indicates average explained variance of all individuals corresponding to the number of principal components and the error bar indicates standard deviation of the explained variance. **d** Linear discriminant analysis was performed 18 times using leave-one-out cross-validation.

the connectivity of a specific ROI was selected for subsequent analyses of classification to narrow down the focus of the analyses to a specific brain region (Fig. 2b). Each ROI was defined based on the automated anatomical labeling template (Tzourio-Mazoyer et al. 2002), which segments the brain into the cerebral cortex (90 regions) and cerebellum (26 regions). In this schematic representation, the left lingual area was the target ROI connected to the seed region (Fig. 2b). Step 3: a principal component analysis was adopted to deal with the high-dimensional data matrix of left M1-based connectivity observed within the left lingual area in each subject (21-by-number of voxels within the ROI) (Fig. 2c). Input data matrix was normalized to have a mean of 0 to obtain the principal components. Principal component analysis reduced the number of voxels within the ROI (2095 voxels within the left lingual area) to a set of orthogonal values (principal components), allowing much of the variance in correlated variables to be explained by a smaller number of components (Weaverdyck et al. 2020). The optimal number of principal components was determined in each ROI according to heuristic criteria; averaging explained variance across individuals was more than 90%, which showed that the optimal number of principal components varied in each ROI in the present study (from 2 to 8, the median value of the optimal number of principal components across ROIs was 5). From steps 1 to 3, individual data were preprocessed. In step 4, each individual's first four loading vectors (in the case of the left lingual area) were concatenated into a matrix to perform linear discriminant analysis with leave-one-out cross-validation to classify the connectivity patterns of V-I, K-I, and ME (Fig. 2d). The loading vectors represent the contribution of each variable to each component or the correlation between a component and a variable to estimate the information they share (Abdi and Williams 2010). In each iteration of cross-validation, a classifier was generated from the training set (all samples minus one) and applied to the test set (left-out sample). This procedure was repeated 18 times, employing data from each individual as a single test set (Keller et al. 1985). Statistical significance was tested using randomly assigned labels (V-I, K-I, and ME) of training data sets, iterated 10,000 times out of 18 repetitions using a permutation test. To calculate the P -value, the null distribution of the average number of correctly predicted labels (with 18 repetitions) was compared to the true average number of correctly predicted labels (with 18 repetitions). The classification was evaluated in terms of sensitivity, specificity, accuracy, and area under the receiver operating characteristic (ROC) curve based on the results of this repetition. The MVPA was performed using MATLAB 2017a (MathWorks, Inc., Natick, MA, USA).

Results

Seed-based Functional Connectivity During V-I, K-I, and ME

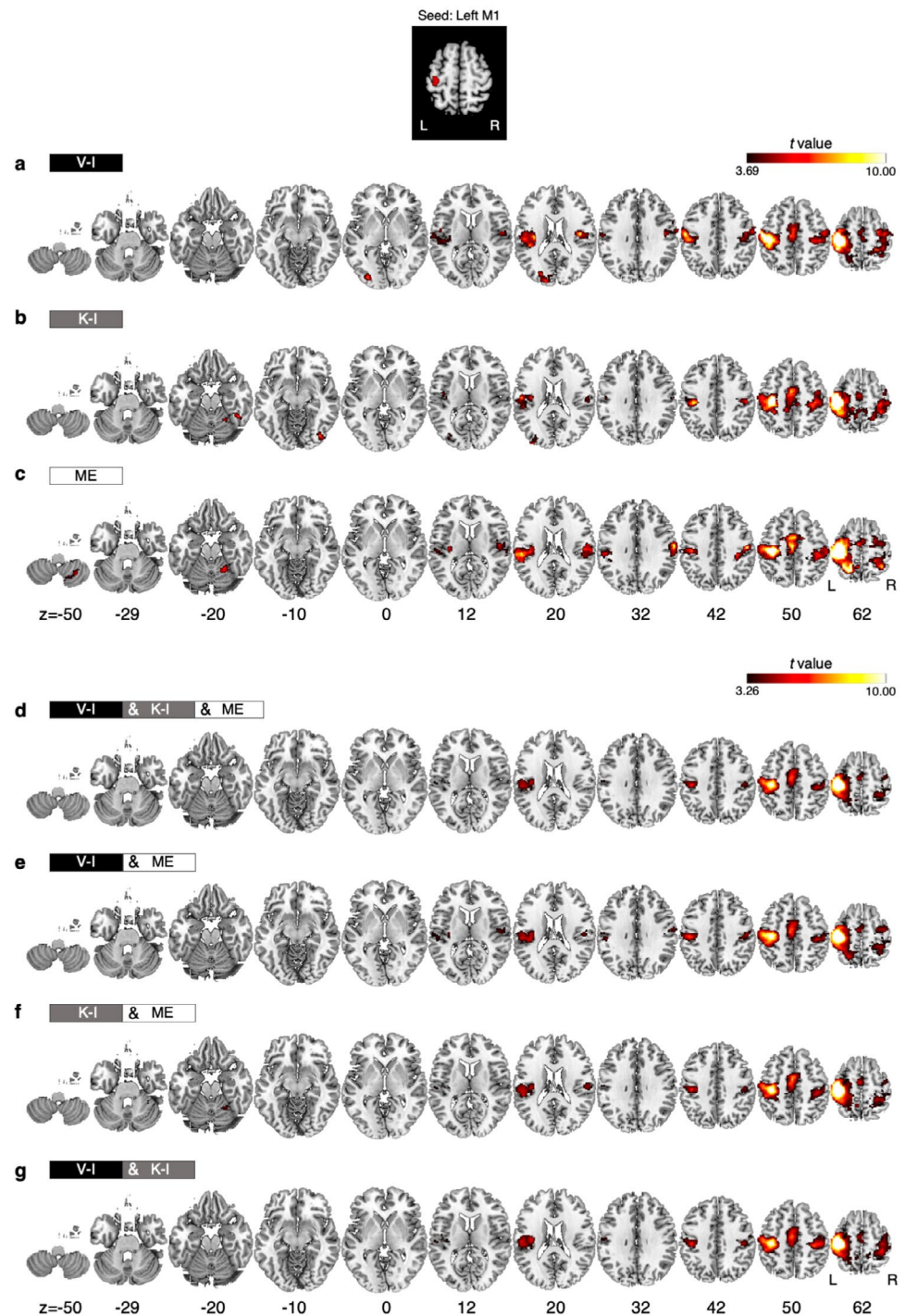
The left M1-based functional connectivity and left SMA-based functional connectivity during V-I, K-I, and ME were constructed (see Supplementary Material Table S1 and Fig. 3a-c for left M1-based functional connectivity; Supplementary Material Table S2 and Fig. S1a-c for left SMA-based functional connectivity; uncorrected $P < 0.001$ with cluster-based FWE rate correction $P < 0.05$).

When the seed region was the left M1, shared functional connectivity among V-I, K-I, and ME was observed across the frontoparietal and temporal areas, including the left M1, bilateral precentral areas, postcentral areas extending to the left precuneus and superior parietal region, supplementary motor areas, left paracentral lobule, superior temporal area, insula extending to the supramarginal gyrus, and Rolandic operculum (Table 1; Fig. 3d). Shared functional connectivity between the V-I and ME, and between K-I and ME is shown in Table 1; Fig. 3e and f. Additionally, the right cerebellum VI was observed in the functional connectivity shared between K-I and ME (Table 1; Fig. 3f), which was marginally significant (uncorrected $P < 0.001$ with cluster-based FWE correction $P = 0.052$), and the right M1 was observed in the functional connectivity shared between V-I and K-I (Table 1; Fig. 3g).

Table 2; Fig. 4 show the brain regions that showed significantly different functional connectivity among V-I, K-I, and ME when the seed region was the left M1. Significantly increased functional connectivity was observed in the left cuneus during V-I compared to that during ME, in the left M1 and cerebellum VI during ME compared to V-I, in the left superior frontal area during K-I compared to ME, in the right fusiform area during K-I compared to V-I.

When the seed region was the left SMA, shared functional connectivity among all conditions was observed across the frontoparietal, subcortical, and temporal areas, including the left M1, SMA, superior frontal areas, left paracentral lobule, bilateral precentral areas, postcentral areas extending to the left precuneus, superior and inferior parietal regions, and bilateral supramarginal areas. The left primary auditory cortex, superior temporal area, bilateral cingulate areas, and insula extending to the Rolandic operculum were also observed (Supplementary Material Table S3 and Fig. S1d-g). Shared functional connectivity between V-I and ME, K-I and ME, and V-I and K-I were similar. There was no significant difference between each condition; however, the left pre- and post-central areas showed increased functional connectivity during V-I than during ME (Supplementary Materials Fig. S2).

Fig. 3 Spatial distribution of the left primary motor cortex-based functional connectivity. The connectivity was constructed during **a** visual motor imagery (V-I), **b** kinesthetic motor imagery (K-I), and **c** motor execution (ME). Shared functional connectivity was observed between **d** V-I, K-I, and ME, between **e** V-I and ME, between **f** K-I and ME, and between **g** V-I and K-I. The hot color map represents the brain areas that were positively correlated with the left primary motor cortex. Statistical significance was set at an uncorrected $P < 0.001$, with a cluster-based family-wise error (FWE) threshold of $P < 0.05$, except in the case of **f** K-I and ME, which included a marginally significant similarity with cluster-based FWE threshold $P = 0.052$ for visualizing purpose.



MVPA

The patterns of the left M1-based functional connectivity during V-I, K-I, and ME were classified above chance level in nine ROIs out of all 116 ROIs, including five cerebral areas (right paracentral lobule, left lingual, angular, middle orbitofrontal, and inferior frontal triangular regions) and four cerebellar areas (right cerebellum VI, cerebellum X,

cerebellum crus II, and left cerebellum crus I). Statistical significance was tested over the nine ROIs to confirm that the sum of the correctly predicted labels across all three task conditions was obtained by random chance. The patterns of left M1-based functional connectivity within the right cerebellum VI, cerebellum crus II, and left lingual area were significantly above chance level in V-I, K-I, and ME ($P < 0.05$).

Table 1 Functional connectivity equivalence of the left primary motor cortex during V-I, K-I, and ME (uncorrected $P < 0.001$ with a cluster-based family-wise error rate of corrected $P < 0.05$)

| Anatomical areas | Hemi | All three conditions | | | | | | V-I and ME | | | K-I and ME | | | V-I and K-I | | | | | | |
|--------------------------|------|----------------------|-----|----|---------|-----|-----|-----------------|-------|-----|------------|----|-------|-----------------|-----|----|---------|-----|-----|----|
| | | MNI coordinates | | | t-value | | | MNI coordinates | | | t-value | | | MNI coordinates | | | t-value | | | |
| | | x | y | z | x | y | z | x | y | z | x | y | z | x | y | z | x | y | z | |
| Frontal Lobe | | | | | | | | | | | | | | | | | | | | |
| Primary motor cortex | L | -38 | -24 | 62 | 21.61 | -38 | -24 | 62 | 21.61 | -38 | -24 | 62 | 21.94 | -38 | -24 | 62 | 21.61 | -38 | -24 | 62 |
| | R | | | | | | | | | | | | | | | | | | | |
| Paracentral lobule | L | -2 | -22 | 52 | 5.32 | | | | | | | | | | | | | | | |
| | R | | | | | | | | | | | | | | | | | | | |
| Precentral cortex | L | -32 | -8 | 68 | 8.17 | -32 | -8 | 68 | 8.17 | -34 | -8 | 68 | 8.42 | -32 | -8 | 68 | 8.17 | -32 | -8 | 68 |
| | R | 34 | -14 | 66 | 4.86 | 36 | -12 | 64 | 5.50 | 34 | -14 | 66 | 4.86 | 34 | -14 | 66 | 5.77 | 34 | -14 | 66 |
| Supplementary motor area | L | -2 | -10 | 52 | 6.70 | -2 | -10 | 52 | 6.97 | 0 | -4 | 52 | 7.74 | -4 | -12 | 50 | 6.79 | -4 | -12 | 50 |
| | R | | | | | | | | | | | | | | | | | | | |
| Rolandic operculum | L | -38 | -30 | 22 | 3.84 | -46 | -26 | 22 | 5.56 | -38 | -30 | 22 | 3.84 | -38 | -30 | 22 | 3.84 | -38 | -30 | 22 |
| | R | | | | | | | | | | | | | | | | | | | |
| Subcortical Areas | | | | | | | | | | | | | | | | | | | | |
| Insula | L | -36 | -18 | 18 | 5.53 | -36 | -18 | 18 | 5.53 | -36 | -18 | 18 | 5.53 | -36 | -18 | 20 | 5.97 | -36 | -18 | 20 |
| Temporal Lobe | | | | | | | | | | | | | | | | | | | | |
| Superior temporal area | L | -54 | -34 | 24 | 3.53 | -54 | -34 | 24 | 3.53 | -62 | -30 | 14 | 4.04 | -54 | -34 | 24 | 3.53 | -54 | -34 | 24 |
| Parietal Lobe | | | | | | | | | | | | | | | | | | | | |
| Postcentral cortex | L | -52 | -16 | 52 | 7.49 | -46 | -20 | 50 | 9.42 | -32 | -42 | 58 | 8.18 | -50 | -20 | 50 | 7.14 | -50 | -20 | 50 |
| | R | 46 | -28 | 54 | 5.85 | 38 | -28 | 48 | 5.87 | 42 | -30 | 54 | 6.14 | 42 | -24 | 54 | 6.33 | 42 | -24 | 54 |
| Precuneus | L | -10 | -48 | 60 | 4.08 | -8 | -50 | 64 | 3.73 | -8 | -50 | 64 | 5.00 | -10 | -48 | 60 | 4.08 | -10 | -48 | 60 |
| Superior parietal lobule | L | -30 | -46 | 66 | 5.53 | -20 | -56 | 62 | 5.80 | -20 | -46 | 66 | 5.99 | -30 | -46 | 66 | 5.53 | -30 | -46 | 66 |
| | R | | | | | | | | | | | | | | | | | | | |
| Supramarginal area | L | -52 | -26 | 22 | 5.27 | -54 | -24 | 20 | 5.24 | -52 | -28 | 22 | 6.09 | -54 | -20 | 18 | 5.79 | -54 | -20 | 18 |
| Cerebellum | | | | | | | | | | | | | | | | | | | | |
| Cerebellum VI* | R | | | | | | | | | | | | | | | | | | | |

Abbreviations: V-I, visual motor imagery; K-I, kinesthetic motor imagery; ME, motor execution; L, left; R, right *The cerebellum VI was marginally significant (cluster-based family-wise error rate: corrected $P = 0.052$).

Table 2 Significant difference in the left primary motor cortex-based functional connectivity between visual motor imagery, kinesthetic motor imagery, and motor execution conditions

| Contrast | Cluster | Cluster | Peak T | MNI coordinates | | | Region |
|--|-------------|---------|--------|-----------------|-----|-----|-----------------------|
| | p(FWE-corr) | | | x | y | z | |
| Visual motor imagery > Motor execution | 0.018 | 99 | 4.96 | -14 | -80 | 30 | Cuneus |
| | | | 4.13 | -24 | -82 | 30 | Cuneus |
| | | | 4.04 | -6 | -82 | 28 | Cuneus |
| Motor execution > Visual motor imagery | 0.050 | 80 | 7.84 | -32 | -22 | 66 | Primary motor cortex |
| | | | 4.54 | -36 | -28 | 62 | Postcentral cortex |
| | 0.017 | 100 | 7.19 | -40 | -50 | -24 | Cerebellum VI |
| | | | 6.90 | -32 | -56 | -24 | Cerebellum VI |
| Kinesthetic motor imagery > Motor execution | 0.012 | 109 | 5.78 | -6 | 46 | 46 | Superior frontal area |
| | | | 4.74 | -6 | 38 | 40 | Medial frontal area |
| | | | 4.74 | -2 | 38 | 54 | Superior frontal area |
| Motor execution > Kinesthetic motor imagery | None | | | | | | |
| Visual motor imagery > Kinesthetic motor imagery | None | | | | | | |
| Kinesthetic motor imagery > Visual motor imagery | 0.038 | 85 | 5.52 | 42 | -50 | -22 | Fusiform |
| | | | 5.32 | 38 | -42 | -24 | Fusiform |

Table 3 Sensitivity, specificity, accuracy, and area under the receiver operating characteristic (ROC) curve for each condition

| Seed region | Region | Condition | Sensitivity | Specificity | Accuracy | Area under the ROC curve |
|-------------------------------|-------------------------------|-----------|-------------|-------------|----------|--------------------------|
| Left primary motor cortex | Right cerebellum VI | V-I | 0.41 | 0.67 | 0.58 | 0.63 |
| | | K-I | 0.40 | 0.71 | 0.60 | |
| | | ME | 0.35 | 0.70 | 0.58 | |
| | Right cerebellum crus II | V-I | 0.38 | 0.72 | 0.61 | 0.64 |
| | | K-I | 0.40 | 0.71 | 0.61 | |
| | | ME | 0.43 | 0.67 | 0.59 | |
| | Left lingual | V-I | 0.37 | 0.68 | 0.57 | 0.63 |
| | | K-I | 0.36 | 0.71 | 0.59 | |
| | | ME | 0.42 | 0.69 | 0.60 | |
| Left supplementary motor area | Right putamen | V-I | 0.42 | 0.68 | 0.59 | 0.71 |
| | | K-I | 0.38 | 0.71 | 0.60 | |
| | | ME | 0.40 | 0.71 | 0.60 | |
| | Right thalamus | V-I | 0.38 | 0.72 | 0.61 | 0.68 |
| | | K-I | 0.37 | 0.68 | 0.58 | |
| | | ME | 0.41 | 0.68 | 0.59 | |
| | Right cerebellum IV-V | V-I | 0.34 | 0.74 | 0.61 | 0.64 |
| | | K-I | 0.37 | 0.64 | 0.55 | |
| | | ME | 0.45 | 0.70 | 0.62 | |
| | Left superior parietal lobule | V-I | 0.38 | 0.75 | 0.63 | 0.68 |
| | | K-I | 0.38 | 0.71 | 0.60 | |
| | | ME | 0.44 | 0.64 | 0.57 | |

V-I, Visual motor imagery; K-I, Kinesthetic motor imagery; ME, Motor execution

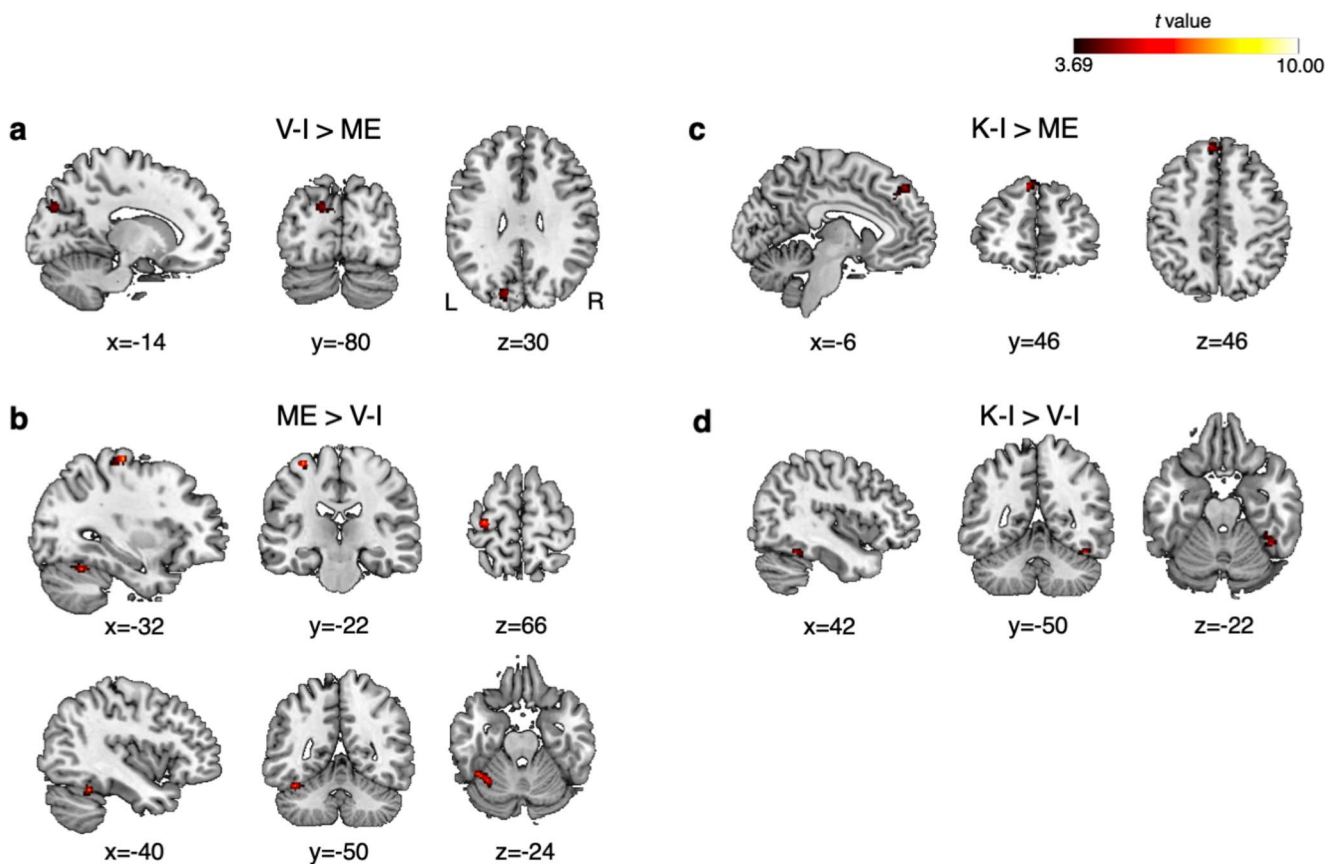


Fig. 4 Difference in the left primary motor cortex-based functional connectivity among visual motor imagery (V-I), kinesthetic motor imagery (K-I), and motor execution (ME). The brain regions that had significantly increased connectivity with the left primary motor

cortex are represented as red **a** during V-I compared to ME, **b** during ME compared to V-I, **c** during K-I compared to ME, and **d** during K-I compared to V-I. Statistical significance was set at an uncorrected $P < 0.001$, with a cluster-based family-wise error threshold $P < 0.05$.

The patterns of the left SMA-based functional connectivity during V-I, K-I, and ME were classified above chance level in five ROIs, including right putamen, thalamus, cerebellum IV-V, vermis IV-V, and left superior parietal lobule. Statistical significance was also tested over the five ROIs, revealing that the connectivity patterns within the right putamen, thalamus, cerebellum IV-V, and left superior parietal lobule were classified above chance level across the conditions ($P < 0.05$).

The classification results, including a confusion matrix for correct and incorrect classification rates across the three task conditions and information on the sensitivity, specificity, accuracy, and area under the ROC curve, are described in Supplementary Material Fig. S3 and Table 3. The patterns of seed-based functional connectivity observed within the ROIs are illustrated in Supplementary Material Fig. S4 and S5.

Discussion

The present study focused on left M1-based functional connectivity with the whole-brain area to identify the network equivalence and difference during target-oriented V-I, K-I, and ME. The frontoparietal and temporal areas, including the bilateral sensorimotor cortices, were all involved in the M1-based functional connectivity during each condition. Regarding different functional networks, increased functional connectivity was observed in the left cuneus during V-I compared to ME, the left superior frontal area during K-I compared to ME, the right fusiform area during K-I compared to V-I, and cerebellum VI during ME compared to V-I. In addition, we investigated left SMA-based functional connectivity across the conditions and found similar results to those of M1-based connectivity. No significant difference was observed between the conditions except that the left pre- and post-central areas showed increased connectivity during V-I than during ME when the seed region was the left SMA. Therefore, in the present study, we mainly discussed the results of M1-based functional connectivity with

the whole-brain area based on the above findings. MVPA results showed that motor imagery and ME were classified using the spatial patterns of M1-based functional connectivity within the right cerebellum VI, cerebellum crus II, and left lingual area and using the spatial patterns of SMA-based functional connectivity within the right putamen, thalamus, cerebellar IV-V, and left superior parietal lobule.

Equivalent Functional Connectivity in V-I, K-I, and ME

In this study, we observed that the M1 and SMA were functionally connected with the frontoparietal and temporal areas during V-I, K-I, and ME. As target-oriented motor imagery is the mental rehearsal of ME without overt activation, it requires cognitive processes, such as motor planning and preparations (Munzert et al. 2009). Therefore, activation of the frontoparietal areas during motor imagery and ME may represent emulated actions (Ptak et al. 2017) to decode motor representation of the movement goal (Gertz et al. 2017). The finding was consistent with that reported in previous studies (Grezes and Decety 2001; Hetu et al. 2013), indicating that functional connections between the M1 and frontoparietal areas are prerequisite states of both motor imagery and ME. In particular, internal representation of target-oriented actions may lead to active recruitment of dorsal frontoparietal network (Ptak et al. 2017). Additionally, functional connectivity with the temporal areas may be induced by auditory stimulation during the experiment, which is consistent during motor imagery and execution.

Different Functional Connectivity Among V-I, K-I, and ME

Functional connections observed only during motor imagery

We observed that the left M1 had no apparent functional connection with the right M1 (i.e., ipsilateral M1) during ME but had significant connections during both V-I and K-I. In the previous studies, ipsilateral sensorimotor activation during simple hand movement was absent or weak (S.-G. Kim et al., 1993; Kobayashi, Hutchinson, Schlaug, & Pascual-Leone, 2003) by means of interhemispheric inhibition (Kobayashi et al. 2003). In contrast, bilateral activations were observed to a greater extent in the sensorimotor cortices during motor imagery than during ME (Batula et al. 2017). Inhibition of superfluous brain activation of the ipsilateral M1 may be unnecessary for motor imagery in the absence of external motor movement.

Similarly, left M1-based functional connection with occipital areas was observed during V-I and K-I, but not during ME. Because no visual input was provided for the participants with closed eyes during the fMRI experiment, this phenomenon would have reflected the nature of motor imagery tasks per se. During both target-oriented motor imagery, internal representation occurred including aiming, and grasping and releasing of the target objects (Lee et al. 2019). Therefore, functional connectivity between the M1 and occipital area was strengthened more during motor imagery than during ME, which may require less visual information to be performed.

Functional connections observed only during K-I and ME

Our findings suggest that the M1-based functional cerebellar connection of K-I mimics that of ME, but V-I did not. The cerebellum regions included the right cerebellum VI during K-I and ME, as well as the right cerebellum VIII and vermis lobule VIII during ME. It has been suggested that the cerebellum takes part in the modulation of internal representation of motor movement by forward model implemented in the region (Grush 2004). The neural processing of this forward model included the use of proprioception/kinesthetic information to achieve desired motor output (Grush 2004). Besides its role in motor control, the cerebellum was also reported to be involved in processing sensory information, especially human kinesthesia (Gao et al. 1996; Naito et al. 2002). Additionally, the cerebellum may inhibit motor output activity during K-I, as shown in a previous study where the increase in motor-evoked potentials during motor imagery disappeared after anodal cerebellar transcranial direct current stimulation (Cengiz and Boran 2016).

Functional connections observed only during V-I

Compared to during ME, increased functional connectivity of the left cuneus was observed during V-I but was not evident during K-I. Since the cuneus is the primary visual area involved in cardinal visual processing (Tong 2003), the finding supports that basic visual processing is interconnected with the motor network during V-I. It was consistent with a previous study, the stronger functional network during V-I was associated with occipital areas, including the cuneus (Solodkin et al. 2004).

Functional connections observed only during K-I

During target-oriented K-I, increased M1-based functional connectivity with the right fusiform was observed compared to V-I. The fusiform is involved in self-other

discrimination (Vocks et al. 2010), raising the possibility that K-I may require the participants to be more self-aware than V-I. In addition, compared to ME, M1-based connectivity was increased with the left superior frontal area during K-I, which has been recognized as a “core self” area (Gusnard et al. 2001; Voegeley and Fink 2003). The finding may highlight that internal representation is considerably more important during K-I than during ME. Because the participants repeated actual hand grasping and releasing toward an imagined target at fixed intervals without any visual stimuli, self-awareness may be relatively less required during ME (Blakemore and Frith 2003). On the other hand, kinesthetic sensation may influence the sense of body ownership, contributing to self-awareness (Walsh et al. 2011). The results can be potentially helpful in elucidating the effect of K-I training in enhancing self-awareness of body movements in patients with spatial neglect after brain injury.

Different Patterns of Functional Connectivity Among V-I, K-I, and ME

MVPA is based on the simple phenomenon that patterns of neural activity are valuable because they contain information about cognitive states (Norman et al. 2006). Instead of focusing on isolated voxels individually, it allows researchers to identify patterns represented in different brain structures. A more direct statistical approach, such as analysis of variance, may provide direct evidence, although it is a univariate test that does not consider distributed information encoded within specific locations (Treder 2020). Furthermore, MVPA has also been applied to analyze patterns of brain functional connectivity. Previous studies have shown that it can successfully predict individual brain maturity (Dosenbach et al. 2010) or discriminate patients from controls (Dosenbach et al. 2010; Liu et al. 2015). In the present study, MVPA was adopted to investigate the brain areas that can significantly discriminate V-I, K-I, and ME based on the patterns of seed-based functional connectivity. Using the pre-defined ROIs, we independently narrowed the focus of the analyses to specific brain regions. When the seed region was the left M1, three brain areas were classified significantly above chance level: the right cerebellum VI, cerebellum crus II, and left lingual region. This may imply that the patterns of M1-based functional connectivity during motor imagery and ME are similar in most brain areas, except in the cerebellar and visual regions, which is consistent with the aforementioned univariate results. When the seed region was the left SMA, four brain areas were significantly classified above chance level: the right putamen, thalamus, cerebellar areas IV-V, and left superior parietal lobule. These observed regions were all engaged in the motor learning

process (Hardwick et al. 2013). The univariate connectivity analysis revealed no significant difference in these areas among the three conditions; however, the findings indicate that the sensorimotor network may have different topological organizations during motor imagery and ME. Therefore, the results of MVPA suggest that patterns of M1- and SMA-based functional connectivity with whole-brain areas show both functional equivalence and differences during the V-I, K-I, and ME, and the spatially distributed patterns of functional connectivity within the specific brain areas can be used to decode the mental state of individuals performing these motor tasks.

Limitation

There are several limitations to the present study. First, we could not confirm that no movement occurred during motor imagery in the fMRI experiment. However, detailed instructions and opportunities to practice motor imagery without any hand motion using surface electromyography were provided to the participants during the motor imagery training sessions. Second, the contralateral M1 and SMA were determined as the seed region in this study; thus, the results should be interpreted within the range of functional connectivity based on the seed regions. Third, differences in the functional connectivity between the dominant and non-dominant sides were not investigated because the grasping and releasing of motor imagery and ME were executed with only the dominant hand. Further studies are necessary to investigate whether the seed-based functional connectivity is lateralized by identifying functional connectivity during both motor imagery and ME performing hand movements on both sides. Finally, the small sample size may lead to a lack of power to detect subtle differences between conditions. In particular, MVPA should include enough samples for each condition to reliably calculate the typical activation (in this study, connection) within each voxel per condition (Weaverdyck et al. 2020). Because the MVPA aimed to classify connectivity patterns between different types of motor imagery and ME, which we expected to be very similar in each condition, more trials per participant are needed in a future study to obtain robust classification results (Weaverdyck et al. 2020). A large sample with adequate statistical power would be warranted in future studies.

Conclusions

The present study demonstrated functional equivalence and differences among V-I, K-I, and ME during target-oriented grasping actions of the right hand. There was shared left

M1-functional connectivity with the bilateral frontoparietal and temporal areas and different functional connectivity with the fronto-occipital and cerebellar areas. There was shared left SMA-based functional connectivity with the bilateral frontoparietal and temporal areas extending to the subcortical regions during V-I, K-I, and ME. In the MVPA, V-I, K-I, and ME could be differentiated in terms of the spatially distributed patterns of functional connectivity within the right cerebellum VI, cerebellum crus II, and left lingual area when the seed region was left M1 and within the right putamen, thalamus, cerebellar areas IV-V, and left superior parietal lobule when the seed region was the left SMA. Fine-grained spatial representation of functional connectivity patterns will be helpful in successfully discriminating V-I, K-I, and ME. These results emphasize the importance of motor-related functional connectivity and its patterns, providing novel insights into how subtypes of motor imagery can be performed from a network perspective.

Supplementary Information The online version contains supplementary material available at <https://doi.org/10.1007/s10548-023-00956-x>.

Author Contribution Eunkyung Kim: Conceptualization, Methodology, Software, Formal analysis, Investigation, Data Curation, Writing – Original Draft, Visualization. Woo Hyung Lee: Conceptualization, Methodology, Software, Investigation, Data Curation, Writing – Original Draft. Han Gil Seo: Conceptualization, Resources, Methodology, Writing – Review & Editing. Hyung Seok Nam: Resources, Methodology, Writing – Review & Editing. Yoon Jae Kim: Resources, Data Curation, Writing – Review. Min-Gu Kang: Resources, Data Curation, Writing – Review. Moon Suk Bang: Conceptualization, Resources, Methodology, Software, Project administration, Funding acquisition, Writing – Review & Editing. Sungwan Kim: Conceptualization, Resources, Methodology, Software, Writing – Review & Editing. Byung-Mo Oh: Conceptualization, Resources, Methodology, Software, Writing – Review & Editing.

Funding This work was supported by the Brain Research Program through the National Research Foundation of Korea (NRF) funded by the Ministry of Science, ICT & Future Planning (2016M3C7A1904984).

Data Availability The datasets generated during and/or analyzed during the current study are available from the corresponding author on reasonable request.

Declarations

Ethics approval This study was performed in line with the principles of the Declaration of Helsinki. Approval was obtained from the Institutional Review Board of Seoul National University Hospital (Ethics approval number: 1707-154-874).

Consent to Participate Informed Consent was obtained from all individual participants included in the study.

Competing interest The authors declare that the research was conducted without any commercial or financial relationships that could be construed as a potential conflict of interest.

References

- Abdi H, Williams LJ (2010) Principal component analysis. *Wiley Interdiscip Rev Comput Stat* 2(4):433–459
- Batula AM, Mark JA, Kim YE, Ayaz H (2017) Comparison of Brain Activation during Motor Imagery and Motor Movement Using fNIRS. *Comput Intell Neurosci*, 2017, 5491296
- Behzadi Y, Restom K, Liao J, Liu TT (2007) A component based noise correction method (CompCor) for BOLD and perfusion based fMRI. *NeuroImage* 37(1):90–101
- Blakemore SJ, Frith C (2003) Self-awareness and action. *Curr Opin Neurobiol* 13(2):219–224
- Cengiz B, Boran HE (2016) The role of the cerebellum in motor imagery. *Neurosci Lett* 617:156–159
- Chen H, Yang Q, Liao W, Gong Q, Shen S (2009) Evaluation of the effective connectivity of supplementary motor areas during motor imagery using Granger causality mapping. *NeuroImage* 47(4):1844–1853
- Cunnington R, Windischberger C, Deecke L, Moser E (2002) The preparation and execution of self-initiated and externally-triggered movement: a study of event-related fMRI. *NeuroImage* 15(2):373–388
- Daly JJ, Wolpaw JR (2008) Brain–computer interfaces in neurological rehabilitation. *Lancet Neurol* 7(11):1032–1043
- Davis T, LaRocque KF, Mumford JA, Norman KA, Wagner AD, Poldrack RA (2014) What do differences between multi-voxel and univariate analysis mean? How subject-, voxel-, and trial-level variance impact fMRI analysis. *NeuroImage* 97:271–283
- Decety J (1996) The neurophysiological basis of motor imagery. *Behav Brain Res* 77(1–2):45–52
- Dosenbach NU, Nardos B, Cohen AL et al (2010) Prediction of individual brain maturity using fMRI. *Science* 329(5997):1358–1361
- Friston KJ, Worsley KJ, Frackowiak RS, Mazziotta JC, Evans AC (1994) Assessing the significance of focal activations using their spatial extent. *Hum Brain Mapp* 1(3):210–220
- Friston KJ, Williams S, Howard R, Frackowiak RS, Turner R (1996) Movement-related effects in fMRI time-series. *Magn Reson Med* 35(3):346–355
- Gallese V, Lakoff G (2005) The Brain’s concepts: the role of the sensory-motor system in conceptual knowledge. *Cogn Neuropsychol* 22(3):455–479
- Gao JH, Parsons LM, Bower JM, Xiong J, Li J, Fox PT (1996) Cerebellum implicated in sensory acquisition and discrimination rather than motor control. *Science* 272(5261):545–547
- Gao Q, Duan X, Chen H (2011) Evaluation of effective connectivity of motor areas during motor imagery and execution using conditional Granger causality. *NeuroImage* 54(2):1280–1288
- Gertz H, Lingnau A, Fiehler K (2017) Decoding Movement Goals from the Fronto-Parietal Reach Network. *Front Hum Neurosci* 11:84
- Grezes J, Decety J (2001) Functional anatomy of execution, mental simulation, observation, and verb generation of actions: a meta-analysis. *Hum Brain Mapp* 12(1):1–19
- Grush R (2004) The emulation theory of representation: motor control, imagery, and perception. *Behavioural and Brain Sciences*, 27(3), 377–396; discussion 396–442
- Guillot A, Collet C, Nguyen VA, Malouin F, Richards C, Doyon J (2009) Brain activity during visual versus kinesthetic imagery: an fMRI study. *Hum Brain Mapp* 30(7):2157–2172
- Gusnard DA, Akbudak E, Shulman GL, Raichle ME (2001) Medial prefrontal cortex and self-referential mental activity: relation to a default mode of brain function. *Proc Natl Acad Sci U S A* 98(7):4259–4264

- Guye M, Parker GJ, Symms M et al (2003) Combined functional MRI and tractography to demonstrate the connectivity of the human primary motor cortex in vivo. *NeuroImage* 19(4):1349–1360
- Hanakawa T, Immisch I, Toma K, Dimyan MA, Van Gelderen P, Hallett M (2003) Functional properties of brain areas associated with motor execution and imagery. *J Neurophysiol* 89(2):989–1002
- Hanakawa T, Parikh S, Bruno MK, Hallett M (2005) Finger and face representations in the ipsilateral precentral motor areas in humans. *J Neurophysiol* 93(5):2950–2958
- Hardwick RM, Rottschy C, Miall RC, Eickhoff SB (2013) A quantitative meta-analysis and review of motor learning in the human brain. *NeuroImage* 67:283–297
- Hardwick RM, Caspers S, Eickhoff SB, Swinnen SP (2018) Neural correlates of action: comparing meta-analyses of imagery, observation, and execution. *Neurosci Biobehav Rev* 94:31–44
- Hetu S, Gregoire M, Saimpont A et al (2013) The neural network of motor imagery: an ALE meta-analysis. *Neurosci Biobehav Rev* 37(5):930–949
- Jeannerod M (1994) The representing brain - neural Correlates of Motor Intention and Imagery. *Behav Brain Sci* 17(2):187–202
- Keller JM, Gray MR, Givens JA (1985) A fuzzy K-Nearest neighbor algorithm. *IEEE Trans Syst Man Cybern Syst* 15(4):580–585
- Kim SG, Ashe J, Hendrich K et al (1993) Functional magnetic resonance imaging of motor cortex: hemispheric asymmetry and handedness. *Science* 261(5121):615–617
- Kim Y, Park E, Lee A, Im C, Kim Y (2018) Changes in network connectivity during motor imagery and execution. *PLoS One*, 13(1), e0190715
- Kobayashi M, Hutchinson S, Schlaug G, Pascual-Leone A (2003) Ipsilateral motor cortex activation on functional magnetic resonance imaging during unilateral hand movements is related to inter-hemispheric interactions. *NeuroImage* 20(4):2259–2270
- Ladda AM, Lebon F, Lotze M (2021) Using motor imagery practice for improving motor performance—a review. *Brain Cogn* 150:105705
- Lee WH, Kim E, Seo HG et al (2019) Target-oriented motor imagery for grasping action: different characteristics of brain activation between kinesthetic and visual imagery. *Sci Rep* 9(1):12770
- Liu F, Guo W, Fouche JP et al (2015) Multivariate classification of social anxiety disorder using whole brain functional connectivity. *Brain Struct Funct* 220(1):101–115
- Mokienko O, Chernikova L, Frolov A, Bobrov P (2014) Motor imagery and its practical application. *Neurosci Behav Physiol* 44(5):483–489
- Munzert J, Lorey B, Zentgraf K (2009) Cognitive motor processes: the role of motor imagery in the study of motor representations. *Brain Res Rev* 60(2):306–326
- Naito E, Kochiyama T, Kitada R et al (2002) Internally simulated movement sensations during motor imagery activate cortical motor areas and the cerebellum. *J Neurosci* 22(9):3683–3691
- Nichols T, Brett M, Andersson J, Wager T, Poline JB (2005) Valid conjunction inference with the minimum statistic. *NeuroImage* 25(3):653–660
- Norman KA, Polyn SM, Detre GJ, Haxby JV (2006) Beyond mind-reading: multi-voxel pattern analysis of fMRI data. *Trends Cogn Sci* 10(9):424–430
- Pilgramm S, de Haas B, Helm F et al (2016) Motor imagery of hand actions: decoding the content of motor imagery from brain activity in frontal and parietal motor areas. *Hum Brain Mapp* 37(1):81–93
- Power JD, Schlaggar BL, Petersen SE (2015) Recent progress and outstanding issues in motion correction in resting state fMRI. *NeuroImage* 105:536–551
- Ptak R, Schnider A, Fellrath J (2017) The dorsal Frontoparietal Network: a Core System for emulated action. *Trends Cogn Sci* 21(8):589–599
- Scott SH (2003) The role of primary motor cortex in goal-directed movements: insights from neurophysiological studies on non-human primates. *Curr Opin Neurobiol* 13(6):671–677
- Silver MA, Kastner S (2009) Topographic maps in human frontal and parietal cortex. *Trends Cogn Sci* 13(11):488–495
- Solodkin A, Hlustik P, Chen EE, Small SL (2004) Fine modulation in network activation during motor execution and motor imagery. *Cereb Cortex* 14(11):1246–1255
- Tong F (2003) Primary visual cortex and visual awareness. *Nat Rev Neurosci* 4(3):219–229
- Treder MS (2020) MVPA-Light: a classification and regression toolbox for Multi-Dimensional Data. *Front Neurosci* 14:289
- Tzourio-Mazoyer N, Landeau B, Papathanassiou D et al (2002) Automated anatomical labeling of activations in SPM using a macroscopic anatomical parcellation of the MNI MRI single-subject brain. *NeuroImage* 15(1):273–289
- Vocks S, Busch M, Gronemeyer D, Schulte D, Herpertz S, Suchan B (2010) Differential neuronal responses to the self and others in the extrastriate body area and the fusiform body area. *Cogn Affect Behav Neurosci* 10(3):422–429
- Vogele K, Fink GR (2003) Neural correlates of the first-person-perspective. *Trends Cogn Sci* 7(1):38–42
- Walsh LD, Moseley GL, Taylor JL, Gandevia SC (2011) Proprioceptive signals contribute to the sense of body ownership. *J Physiol* 589(Pt 12):3009–3021
- Weaverdyck ME, Lieberman MD, Parkinson C (2020) Tools of the Trade Multivoxel pattern analysis in fMRI: a practical introduction for social and affective neuroscientists. *Soc Cogn Affect Neurosci* 15(4):487–509
- Whitfield-Gabrieli S, Nieto-Castanon A (2012) Conn: a functional connectivity toolbox for correlated and anticorrelated brain networks. *Brain Connect* 2(3):125–141
- Zabicki A, de Haas B, Zentgraf K, Stark R, Munzert J, Kruger B (2017) Imagined and executed actions in the Human Motor System: testing neural similarity between execution and imagery of actions with a Multivariate Approach. *Cereb Cortex* 27(9):4523–4536

Publisher's Note Springer Nature remains neutral with regard to jurisdictional claims in published maps and institutional affiliations.

Springer Nature or its licensor (e.g. a society or other partner) holds exclusive rights to this article under a publishing agreement with the author(s) or other rightsholder(s); author self-archiving of the accepted manuscript version of this article is solely governed by the terms of such publishing agreement and applicable law.